[11] Labauge P, Horzinski L, Ayrignac X, Blanc P, Vukusic S, Rodriguez D, et al. Natural history of adult-onset eIF2B-related disorders: a multi-centric survey of 16 cases. Brain 2009;132:2161–9.
[12] Wu Y, Pan Y, Du L, Wang J, Gu Q, Gao Z, et al. Identification of novel EIF2B mutations in Chinese patients with vanishing white matter disease. J Hum Genet 2009;54:74–7.
[13] Leng X, Wu Y, Wang X, Pan Y, Wang J, Li J, et al. Functional analysis of recently identified mutations in eukaryotic translation initiation factor 2Bε (eIF2Bε) identified in Chinese patients with vanishing white matter disease. J Hum Genet 2011;56:300–5.
[14] Matsukawa T, Wang X, Liu R, Wortham N, Onuki Y, Kubota A, et al. Adult-onset leukoencephalopathies with vanishing white matter with novel missense mutations in EIF2B2, EIF2B3, and EIF2B5. Neurogenetics 2011;12:259–61.
[15] La Piana R, Vanderver A, van der Knaap M, et al. ADult-onset vanishing white matter disease due to a novel eif2b3 mutation. Arch Neurol 2012;69:765–8.
[16] Alsalem A, Shaheen R, Alkuraya FS. Vanishing white matter disease caused by EIF2B2 mutation with the presentation of an adrenoleukodystrophy phenotype. Gene 2012;496:141–3.
[17] van der Knaap MS, Kamphorst W, Barth PG, Kraaijeveld CL, Gut E, Valk J. Phenotypic variation in leukoencephalopathy with vanishing white matter. Neurology 1998;51:540–7.
[18] Yamamoto T, Nanba E, Ninomiya H, Higaki K, Taniguchi M, Zhang H, et al. NPC1 gene mutations in Japanese patients with Niemann–Pick disease type C. Hum Genet 1999;105:10–6.
[19] Shimojima K, Komoike Y, Tohyama J, Takahashi S, Paez MT, Nakagawa E, et al. TULIP1 (RALGAPA1) haploinsufficiency with brain development delay. Genomics 2009;94:414–22.
[20] Kumar P, Henikoff S, Ng PC. Predicting the effects of coding non-synonymous variants on protein function using the SIFT algorithm. Nat Protoc 2009;4:1073–81.
[21] Adzhubei IA, Schmidt S, Peshkin L, Ramensky VE, Gerasimova A, Bork P, et al. A method and server for predicting damaging missense mutations. Nat Methods 2010;7:248–9.
[22] Kircher M, Witten DM, Jain P, O'Roak BJ, Cooper GM, Shendure J. A general framework for estimating the relative pathogenicity of human genetic variants. Nat Genet 2014;46:310–5.
[23] Shimojima K, Narita A, Maegaki Y, Saito A, Furukawa T, Yamamoto T. Whole-exome sequencing identifies a de novo TUBA1A mutation in a patient with sporadic malformations of cortical development: a case report. BMC Res Notes 2014;7:465.
[24] Fogli A, Schiffmann R, Bertini E, Ughetto S, Combes P, Eymard-Pierre E, et al. The effect of genotype on the natural history of eIF2B-related leukodystrophies. Neurology 2004;62:1509–17.
[25] Matsukawa T, Wang X, Liu R, Wortham NC, Onuki Y, Kubota A, et al. Adult-onset leukoencephalopathies with vanishing white matter with novel missense mutations in EIF2B2, EIF2B3, and EIF2B5. Neurogenetics 2011;12:259–61.
[26] Shimada S, Miya K, Oda N, Watanabe Y, Kumada T, Sugawara M, et al. An unmasked mutation of EIF2B2 due to submicroscopic deletion of 14q24.3 in a patient with vanishing white matter disease. Am J Med Genet A 2012;158A:1771–7.
[27] van der Lei HD, Steenweg ME, Barkhof F, de Grauw T, d'Hooghe M, Morton R, et al. Characteristics of early MRI in children and adolescents with vanishing white matter. Neuropediatrics 2012;43:22–6.
[28] Scheper GC, van der Knaap MS, Proud CG. Translation matters: protein synthesis defects in inherited disease. Nat Rev Genet 2007;8:711–23.
[29] Pavitt GD. EIF2B, a mediator of general and gene-specific translational control. Biochem Soc Trans 2005;33:1487–92.
[30] Liu R, van der Lei HD, Wang X, Wortham NC, Tang H, van Berkel CG, et al. Severity of vanishing white matter disease does not correlate with deficits in eIF2B activity or the integrity of eIF2B complexes. Hum Mutat 2011;32:1036–45.
[31] van der Voorn JP, van Kollenburg B, Bertrand G, Van Haren K, Scheper GC, Powers JM, et al. The unfolded protein response in vanishing white matter disease. J Neuropathol Exp Neurol 2005;64:770–5.
[32] Bugiani M, Boor I, Powers JM, Scheper GC, van der Knaap MS. Leukoencephalopathy with vanishing white matter: a review. J Neuropathol Exp Neurol 2010;69:987–96.
[33] Kantor L, Pinchasi D, Mintz M, Hathout Y, Vanderver A, Elroy-Stein O. A point mutation in translation initiation factor 2B leads to a continuous hyper stress state in oligodendroglial-derived cells. PLoS ONE 2008;3:e3783.

Journal of Human Genetics (2015) 60, 631–635

www.nature.com/jhg

SHORT COMMUNICATION

Novel compound heterozygous *LIAS* mutations cause glycine encephalopathy

Yoshinori Tsurusaki[1], Ryuta Tanaka[2], Shino Shimada[3], Keiko Shimojima[3], Masaaki Shiina[4], Mitsuko Nakashima[1], Hirotomo Saitsu[1], Noriko Miyake[1], Kazuhiro Ogata[4], Toshiyuki Yamamoto[3] and Naomichi Matsumoto[1]

Glycine encephalopathy (GCE) is a rare autosomal recessive disorder caused by defects in the glycine cleavage complex. Here we report a patient with GCE and elevated level of glycine in both the serum and the cerebrospinal fluid. Trio-based whole-exome sequencing identified novel compound heterozygous mutations (c.738-2A>G and c.929T>C (p.Met310Thr)) in *LIAS*. To date, three homozygous mutations have been reported in *LIAS*. All previously reported GCE patients also show elevated level of serum glycine. Our data further supports *LIAS* mutations as a genetic cause for GCE.
Journal of Human Genetics (2015) **60,** 631–635; doi:10.1038/jhg.2015.72; published online 25 June 2015

INTRODUCTION

Glycine encephalopathy (GCE) (MIM 605899), also known as nonketotic hyperglycinemia, is a rare autosomal recessive disorder of the glycine cleavage system[1] that results in elevated glycine levels in body fluids. GCE is genetically caused by mutations in *AMT* (MIM 238310), *GLDC* (MIM 238300) or *GCSH* (MIM 238330), which encode T-, P- or H-protein, respectively, and together with L-protein constitute the glycine cleavage enzyme.[2–4] Most GCE patients have *GLDC* mutations.[5] Recently, *GLRX5* (MIM 609588), *BOLA3* (MIM 613183) and *LIAS* (MIM 607031) were identified as causative mutant genes for GCE.[6,7] *LIAS* encodes lipoic acid synthetase, a [4Fe-4S]-type iron–sulfur cluster-dependent enzyme that acts as a prosthetic group on H-protein, which is localized within the mitochondria.[8] *GLRX5* and *BOLA3* are iron–sulfur cluster biosynthesis genes.[8] All GCE patients showed elevated level of glycine in the serum, but it is only slightly increased in the cerebrospinal fluid, or even normal, in some GCE patients.[6] In this study, we report a GCE individual with novel compound heterozygous mutations in *LIAS*.

PATIENTS AND METHODS

Case report

A 21-year-old female patient was born to healthy nonconsanguineous parents. Her birth weight was 2954 g (mean), length 48.5 cm (mean) and occipitofrontal circumference 33.8 cm (75th percentile). Her initial development was normal until 18 months. Her elder sister died of herpes simplex virus encephalitis at the age of 18 months. Her elder brother is healthy.

At the age of 19 months, she suffered from an upper respiratory infection. Three days later, she vomited, became excited and then drowsy, and showed chorea-like involuntary movements. She was instantly admitted to the intensive care unit. Magnetic resonance imaging of the brain showed no abnormality (Figure 1). Her cerebrospinal fluid was examined, which showed normal results. Two weeks later, high blood glycine levels were noted (1545 nmol ml^{-1}, normal range 179–587 nmol ml^{-1}), which are still present (Table 1). Her cerebrospinal fluid glycine levels were also high: 45.5 nmol ml^{-1} (normal range 1.6–19.5 nmol ml^{-1}; Table 1). Ketourine was not found. Three months later, magnetic resonance imaging of the brain showed high-intensity areas at the caudate nucleus and the putamen, which spread into the deep white matter (Figure 1).

At present, her height is 156 cm (25–50th percentile), weight 47.3 kg (10–25th percentile) and the occipitofrontal circumference 52.5 cm (<3rd percentile). She is now bedridden. Tube feeding has been required since 19 months of age. She speaks no meaningful words and shows no eye contact. Myoclonic movements and intractable epilepsy have been observed. Magnetic resonance imaging of the brain shows brain atrophy, especially in the white matter (Figure 1). The institutional review boards of Yokohama City University School of Medicine and Tokyo Women's Medical University approved the study. Informed consent was obtained from the family.

Whole-exome sequencing

DNA from the patient and her parents were analyzed by whole-exome sequencing, as previously described.[9] Genomic DNA was captured using the SureSelect Human All Exon v5 (50 Mb) Kit (Agilent Technologies, Santa Clara, CA, USA). Captured DNA was sequenced on a HiSeq2500 (Illumina, Inc., San Diego, CA, USA) with 101 bp paired-end reads and 7 bp index reads. Image analysis and base calling were performed by sequence control software real-time analysis and CASAVA software (v1.8) (Illumina, Inc.). Quality-controlled reads were mapped to the human reference genome (UCSC hg19, NCBI build 37.1) using Novoalign (v3.00.02; http://www.novocraft.com/products/novoalign/).

[1]Department of Human Genetics, Yokohama City University Graduate School of Medicine, Yokohama, Japan; [2]Department of Child Health, Institute of Clinical Medicine, University of Tsukuba, Ibaraki, Japan; [3]Institute for Integrated Medical Sciences, Tokyo Women's Medical University, Tokyo, Japan and [4]Department of Biochemistry, Yokohama City University Graduate School of Medicine, Yokohama, Japan
Correspondence: Dr N Matsumoto, Department of Human Genetics, Yokohama City University Graduate School of Medicine, 3-9 Fukuura, Kanazawa-ku, Yokohama 236-0004, Japan.
E-mail: naomat@yokohama-cu.ac.jp
Received 6 February 2015; revised 18 May 2015; accepted 28 May 2015; published online 25 June 2015

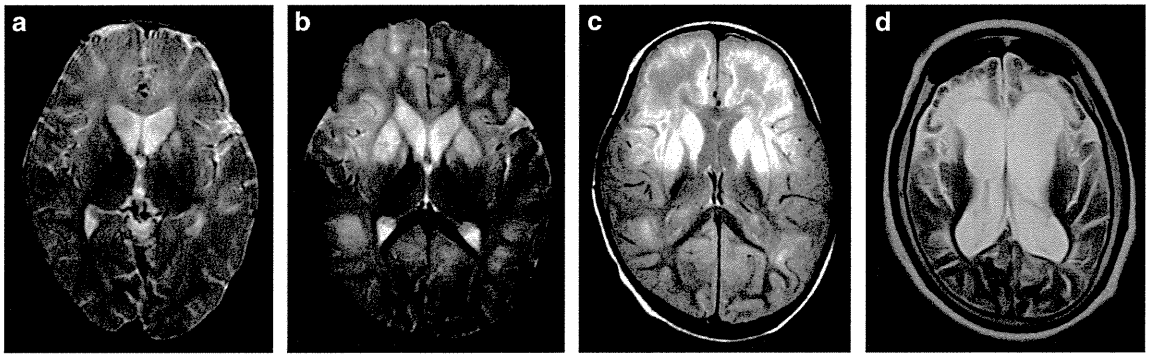

Figure 1 T2-weighted brain magnetic resonance imaging (MRI) of the individual with *LIAS* mutations. (**a**) Examined at disease onset (19 months old). High-intensity areas are present in the caudate nucleus and the putamen. (**b**) Seven days after disease onset. The high-intensity areas have expanded into the white matter, especially in the frontal region. (**c**) One month after disease onset. High-intensity areas are noted not only in the basal nucleus but also in the subcortical white matter, especially in the frontal region. (**d**) At 15 years old. Owing to diffuse cerebral atrophy, the lateral ventricles have expanded. White matter atrophy is predominant in the frontal region.

Table 1 Clinical features of GCE patients with *LIAS* mutations

	This study	*Mayr* et al.,[7]	*Baker* et al.,[6] *(Patient 7)*	*Baker* et al.,[6] *(Patient 8)*
Gene mutation	c.929T>C c.738-2A>G	c.746G>A	c.475_477delGAG insAAA	c.645T>A
Amino acid change	p.M310T Splice site mutation	p.R249H	p.E159K	p.D215E
Plasma glycine (mM; normal range:179–587)	1545	906	890/1035	759
CSF glycine (mM; normal range:1.6–19.5)	45.5	NA	180/94	16
CSF/plasma glycine ratio	0.03	NA	0.20/0.09	0.02
Age	21 Years	4 Years/death	2 Years 8 months/death	14 Years
Onset	19 Months	Third day	Third day	Second day
Initial symptoms	Acute encephalopathy with involuntary movements	Seizure	Hypotonia, seizure	Hypotonia, seizure
Developmental delays	+	NA	+	+
Brain images	Brain atrophy of the especially in the white matter	Multicystic encephalopathy, hydrocephalus *ex vacuo*	Brain atrophy of the cerebrum in both the cortex and the white matter	Normal

Abbreviations: +, present; −, absent; CSF, cerebrospinal fluid; NA, data not available.

After removal of PCR duplications using Picard (v1.55; http://broadinstitute.github.io/picard/), single-nucleotide variants and short insertions and deletions (Indels) were called using Genome Analysis Toolkit (v1.6-5; https://www.broadinstitute.org/gatk/) and were annotated using ANNOVAR (June 2013; http://annovar.openbioinformatics.org/en/latest/).

Prioritization of variants

All variants within exons or ±2 bp from exon–intron boundaries and registered in dbSNP137, the National Heart Lung and Blood Institute Exome Sequencing Project Exome Variant Server (NHLBI-ESP 6500), Human Genome Variation Database, or our in-house (exome data from 575 Japanese individuals) databases, as well as synonymous variants, were removed. Variants were confirmed by Sanger sequencing with an ABI PRISM 3500xl or ABI3130xl autosequencer (Life Technologies, Carlsbad, CA, USA).

Structural modeling

Crystal structure of lipoyl synthase 2 from *Thermosynechococcus elongatus* (PDB code 4U0P)[10] was selected as the most similar model to human LIAS by Phyre2 protein fold recognition server.[11]

Reverse transcription-PCR and nonsense-mediated mRNA decay analysis

Lymphoblastoid cell lines derived from the patient and a healthy control were established. After incubation with 1.5 µl of dimethyl sulfoxide(as a negative control) or 1.5 µl of the protein synthesis inhibitor cycloheximide (100 mg ml^{-1} in dimethyl sulfoxide) (Sigma-Aldrich, St Louis, MO, USA) for 4 h. Total RNA was isolated from treated lymphoblastoid cells using the RNeasy Plus Mini Kit (Qiagen, Hilden, Germany) and was used for reverse transcription with the Super Script III First-Strand Synthesis System (Life Technologies). One microliter of synthesized cDNA was amplified by PCR. PCR products were electrophoresed on a 5%–20% gradient polyacrylamide gel, stained with ethidium bromide and quantitatively measured using a FluorChem 8900 (Alpha Innotech, San Leandro, CA, USA). Three independent experiments were performed. Statistical analyses were performed using analysis of variance. Each PCR band was cloned into the pCR4-TOPO vector (Life Technologies) and sequenced using ABI 3130xl autosequencer.

RESULTS

The mean read depth against RefSeq coding sequence was 89.08–123.7 reads, with 92.2%–94.7% of coding sequence covered by 20 or more

reads. We focused on *de novo* and recessive mutations. We only found novel compound heterozygous mutations in *LIAS*. Sanger sequencing confirmed that c.738-2A>G was transmitted from her mother and c.929T>C (p.Met310Thr) from her father (Figure 2a and Table 1). These two mutations were not registered in dbSNP137, National Heart Lung and Blood Institute Exome Sequencing Project Exome Variant Server (NHLBI-ESP 6500), Human Genome Variation Database, or our in-house 575 Japanese control exome databases. The missense mutation (p.Met310Thr) was predicted as damaging by SIFT (http://sift.jcvi.org/), Polyphen-2 (http://genetics.bwh.harvard.edu/pph2/) and MutationTaster (http://www.mutationtaster.org/), and was evolutionarily conserved (Figure 2a). Moreover, the p.Met310Thr substitution localizes to the Elp3 domain in an iron–sulfur cluster binding site predicted by SMART (http://smart.embl-heidelberg.de/) (Figure 2a). The splice site mutation (c.738-2A>G) was predicted to abolish an acceptor site by ESEfinder (http://rulai.cshl.edu/cgi-bin/tools/ESE3/esefinder.cgi), NetGene2 (http://www.cbs.dtu.dk/services/NetGene2/) and BDGP (http://www.fruitfly.org/seq_tools/splice.html).

We mapped the mutation site (p.Met310Thr) on the crystal structure of lipoyl synthase 2 from *T. elongatus* (TeLipA2) (PDB code 4U0P),[10] analogous to human LIAS (Met310 in human LIAS corresponds to Leu241 in TeLipA2), to evaluate structural impact of the mutation. The main-chain amide and carbonyl groups of Leu241 (Met310) make hydrogen bonds to adenine ring of 5′-methylthioadenosine, a breakdown product of the *S*-adenosylmethionine (Figure 2b), suggesting that the stability of the main-chain region around Leu241 (Met310) is important in *S*-adenosylmethionine binding. The side chain of Leu241 is involved in a hydrophobic core (Figure 2b) and is considered to contribute to the main-chain stability. Thus, the p.Leu241Thr (p.Met310Thr) mutation is likely to impair the enzymatic activity due to destabilized *S*-adenosylmethionine binding.

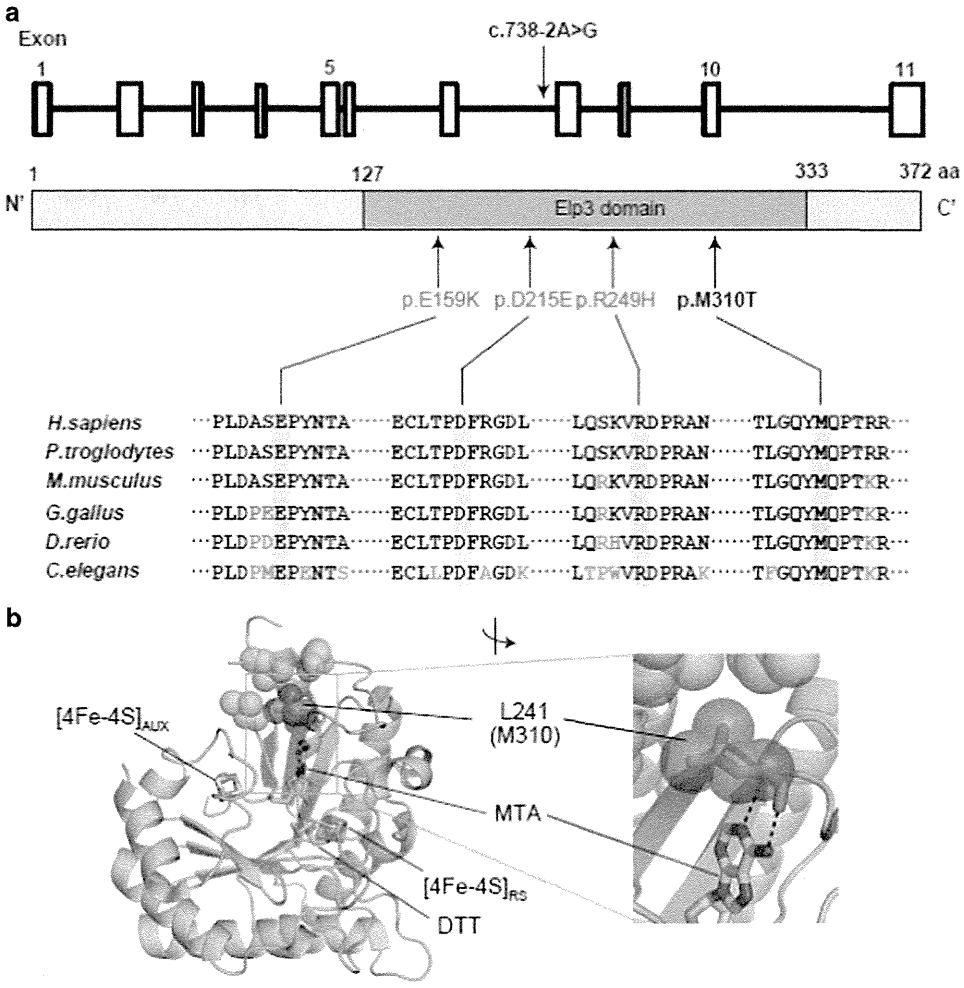

Figure 2 All the *LIAS* mutations. (**a**) *LIAS* missense mutations. Novel compound heterozygous mutations (c.738-2A>G and c.929T>C (p.M310T)) identified in the patient. The upper and middle panels show the *LIAS* gene structure that comprises 11 exons. LIAS contains an Elp3 domain, predicted by SMART. The lower panel shows evolutionary conservation of the mutated amino acid through six different species. The altered nucleotides are highlighted in gray boxes. Three previously reported mutations (p.R249H, p.E159K and p.D215E) are highlighted in gray. (**b**) Mutation mapping on the crystal structure of lipoyl synthase 2 from *T. elongatus* (PDB code 4U0P), which is analogous to human LIAS. The mutation site is shown as sticks with translucent spheres in red in the whole (left) and the close-up (right) views of the enzyme structure. 5′-methylthioadenosine (MTA), [4Fe-4S] clusters and dithiothreitol (DTT) are depicted in color-coded sticks: green for C, red for O, blue for N, yellow for S and orange for Fe. Some hydrophobic side chains forming a core with Leu241 are shown as translucent spheres. The amino acid number in the parentheses is that for human LIAS. Black dashed lines indicate hydrogen bonds. A full color version of this figure is available at the *Journal of Human Genetics* journal online.

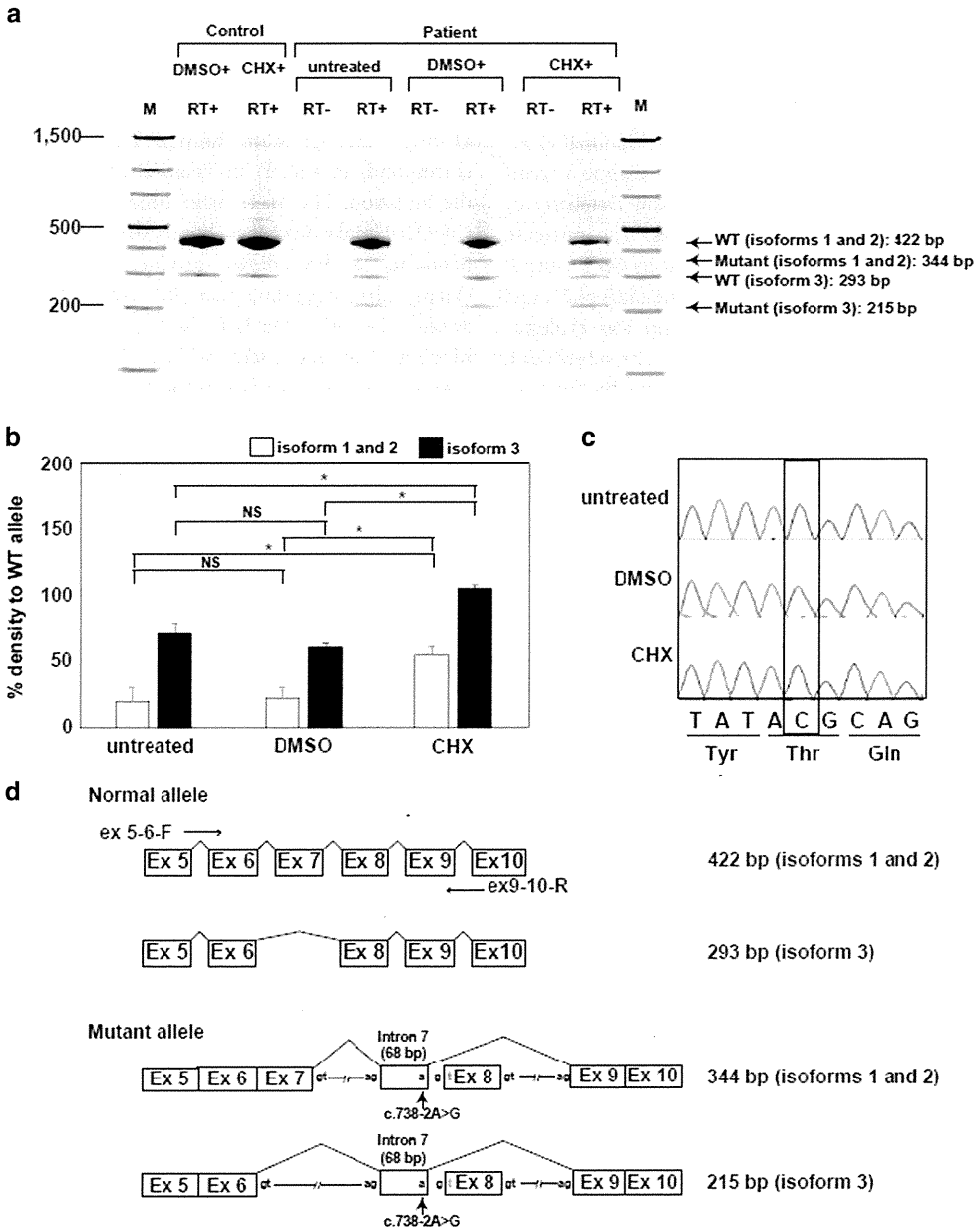

Figure 3 A splice site *LIAS* mutation. (**a**) Reverse transcription-PCR (RT-PCR) analysis showing two PCR products (422-bp (isoforms 1 and 2) and 293-bp (isoform 3)) were observed in a healthy control individual. By contrast, a 344-bp product (corresponding to isoforms 1 and 2) and a 215-bp product (corresponding to isoform 3) were detected in cycloheximide (CHX)-treated cells from the patient at a higher level compared with untreated and dimethyl sulfoxide (DMSO)-treated cells. (**b**) Densitometric data of the RT-PCR products represented as mean ± s.d. $*P<0.05$ by analysis of variance (ANOVA). NS, not significant. (**c**) Sequencing of the 422-bp wild type (WT) product only found missense mutation allele based on the electropherogram. (**d**) Schematic presentation of RT-PCR products. Sequencing of the 344-bp product showed a 68-bp insertion from intron 7 and exon 8 skipping, producing a premature stop codon at amino acid position 250. Sequencing of the 215-bp product showed a 68-bp insertion from intron 7 and exons 7 and 8 skipping, producing a premature stop codon at amino acid position 207. M, molecular size marker; WT, wild type. A full color version of this figure is available at the *Journal of Human Genetics* journal online.

To examine the mutational effects of c.738-2A>G, reverse transcription-PCR was performed. Two PCR products (422-bp (isoforms 1 and 2) and 293-bp (isoform 3)) were observed in a healthy control individual regardless of the cycloheximide treatment (Figure 3a). By contrast, a 344-bp product (corresponding to isoforms 1 and 2) and a 215-bp product (corresponding to isoform 3) were newly detected from cycloheximide-treated cells from the patient at a higher level compared with untreated and dimethyl sulfoxide-treated cells, strongly indicating the abnormally spliced allele was subjected to the nonsense-mediated mRNA decay (Figure 3b). In the 422-bp product, only the missense mutation allele was seen in the electropherograms of all untreated, dimethyl sulfoxide- and cycloheximide-treated cells (Figure 3c). Therefore, the normally spliced allele only contained the missense mutation. Sequencing of the 344-bp product showed a 68-bp insertion from intron 7 and exon 8 skipping, producing a premature stop codon at amino acid position 250

(Figure 3d). In addition, sequencing of the 215-bp product confirmed a 68-bp insertion from intron 7 and exons 7 and 8 skipping, producing a premature stop codon at amino acid position 207 (Figure 3d).

DISCUSSION

We report a family with compound heterozygous mutations (c.738-2A>G and c.929T>C (p.M310T)) in *LIAS*, which showed developmental delays, myoclonic movements and intractable epilepsy (Table 1). Magnetic resonance imaging of the brain showed atrophy in the white matter (Figure 1). The patient also showed late-onset involuntary movements such as chorea and elevated level of glycine in both the serum and the cerebrospinal fluid (Table 1). The splice acceptor site mutation leads to the error in splicing of intron 7 and exon 8, with a premature stop codon at amino acid position 250 in isoforms 1 and 2 or 207 in isoform 3. Consequently, the product of this mutant transcript may be subjected to nonsense-mediated mRNA decay (likely as shown in Figure 3) or produce a truncated protein at the Elp3 domain if translated (less likely).

To date, three homozygous mutations (p.R249H, p.E159K and p.D215E) have been reported in *LIAS* patients (Table 1).[6,7] These three missense mutations occur at evolutionarily conserved amino acids in the Elp3 domain (Figure 2a). The three reported patients show early-onset seizures within the first 2–3 days and elevated plasma glycine levels (Table 1). The patient described here shows no seizures and very late disease onset at age of 19 months (Table 1). The variable clinical features in patients with *LIAS* mutations may be associated with the severity of the functional impact on protein lipoylation.[6]

Lias homozygous knockout mice die at the early implantation stage between 7.5 and 9.5 days post coitum, suggesting that *Lias* is essential for embryonic development.[12] The previously reported *LIAS* mutations are all homozygous missense mutations. Lipoamide reduction of lipoylated proteins was severely reduced in two patients (p.Arg249His and p.Glu159Lys) with early infantile lethality (at 2 and 4 years).[6,7] In contrast, one patient (p.Asp215Glu) with hypotonia and seizures showed constant development and residual lipoylated proteins, suggesting that some lipoic acid synthetase activity is retained. Thus, residual lipoic acid synthetase activity may be correlated with phenotypic severity. On the other hand, a glycine level is elevated in all patients. Thus, serum glycine levels may not be correlated with *LIAS* genotypes. Regardless of some biochemical and clinical data, it is difficult to extract clinical difference between our case of heterozygous mutations and reported cases of homozygous missense mutations due to the limited number of patients ($n=4$). Further accumulation of patients with *LIAS* mutations is needed.

Most GCE patients caused by *GLDC* or *AMT* mutations show hypotonia, lethargy and apnea leading to death in the first few days after birth. If they overcome apnea regaining spontaneous respiration, they develop intractable seizures and intellectual disability.[13] All the four patients with *LIAS* mutations including our patient lived after at least 2 years of age. Therefore, *LIAS* mutant phenotype is relatively milder compared with the common GCE.

The acute onset of encephalopathy in our patient is interesting. We assumed that the stressful condition by the upper respiratory infection would have been the trigger of disease progression as sometimes seen in other cases of vanishing white matter.

In conclusion, we have identified for the first time, a patient with compound heterozygous missense and splice site mutations in *LIAS*. Further analysis of *LIAS*-related patients is needed to delineate the phenotypic spectrum and phenotype–genotype correlation.

CONFLICT OF INTEREST

The authors declare no conflicts of interest.

ACKNOWLEDGEMENTS

We thank the patients and their families for their participation in this study. We also thank Nobuko Watanabe for her excellent technical assistance. This work was supported by the Ministry of Health, Labour and Welfare of Japan; the Japan Society for the Promotion of Science (Grants-in-Aid for Scientific Research (A) (B) (C)); the Takeda Science Foundation; the Japan Science and Technology Agency (the fund for Creation of Innovation Centers for Advanced Interdisciplinary Research Areas Program in the Project for Developing Innovation Systems); the Ministry of Education, Culture, Sports, Science and Technology of Japan (the Strategic Research Program for Brain Sciences); and a Grant-in-Aid for Scientific Research on Innovative Areas (Transcription Cycle).

1 Brenton, J. N. & Rust, R. S. Late-onset nonketotic hyperglycinemia with a heterozygous novel point mutation of the GLDC gene. *Pediatr. Neurol.* **50**, 536–538 (2014).
2 Nanao, K., Okamura-Ikeda, K., Motokawa, Y., Danks, D. M., Baumgartner, E. R., Takada, G. *et al.* Identification of the mutations in the T-protein gene causing typical and atypical nonketotic hyperglycinemia. *Hum. Genet.* **93**, 655–658 (1994).
3 Kure, S., Narisawa, K. & Tada, K. Structural and expression analyses of normal and mutant mRNA encoding glycine decarboxylase: three-base deletion in mRNA causes nonketotic hyperglycinemia. *Biochem. Biophys. Res. Commun.* **174**, 1176–1182 (1991).
4 Koyata, H. & Hiraga, K. The glycine cleavage system: structure of a cDNA encoding human H-protein, and partial characterization of its gene in patients with hyperglycinemias. *Am. J. Hum. Genet.* **48**, 351–361 (1991).
5 Kanekar, S. & Byler, D. Characteristic MRI findings in neonatal nonketotic hyperglycinemia due to sequence changes in GLDC gene encoding the enzyme glycine decarboxylase. *Metab. Brain Dis.* **28**, 717–720 (2013).
6 Baker, P. R. 2nd, Friederich, M. W., Swanson, M. A., Shaikh, T., Bhattacharya, K., Scharer, G. H. *et al.* Variant non ketotic hyperglycinemia is caused by mutations in LIAS, BOLA3 and the novel gene GLRX5. *Brain* **137**, 366–379 (2014).
7 Mayr, J. A., Zimmermann, F. A., Fauth, C., Bergheim, C., Meierhofer, D., Radmayr, D. *et al.* Lipoic acid synthetase deficiency causes neonatal-onset epilepsy, defective mitochondrial energy metabolism, and glycine elevation. *Am. J. Hum. Genet.* **89**, 792–797 (2011).
8 Mayr, J. A., Feichtinger, R. G., Tort, F., Ribes, A. & Sperl, W. Lipoic acid biosynthesis defects. *J. Inherit. Metab. Dis.* **37**, 553–563 (2014).
9 Tsurusaki, Y., Koshimizu, E., Ohashi, H., Phadke, S., Kou, I., Shiina, M. *et al. De novo* SOX11 mutations cause Coffin-Siris syndrome. *Nat. Commun.* **5**, 4011 (2014).
10 Harmer, J. E., Hiscox, M. J., Dinis, P. C., Fox, S. J., Iliopoulos, A., Hussey, J. E. *et al.* Structures of lipoyl synthase reveal a compact active site for controlling sequential sulfur insertion reactions. *Biochem. J.* **464**, 123–133 (2014).
11 Kelley, L. A. & Sternberg, M. J. Protein structure prediction on the Web: a case study using the Phyre server. *Nat. Protoc.* **4**, 363–371 (2009).
12 Yi, X. & Maeda, N. Endogenous production of lipoic acid is essential for mouse development. *Mol. Cell. Biol.* **25**, 8387–8392 (2005).
13 Hennermann, J. B., Berger, J. M., Grieben, U., Scharer, G. & Van Hove, J. L. Prediction of long-term outcome in glycine encephalopathy: a clinical survey. *J. Inherit. Metab. Dis.* **35**, 253–261 (2012).

Journal of the Neurological Sciences 351 (2015) 211–213

Contents lists available at ScienceDirect

Journal of the Neurological Sciences

journal homepage: www.elsevier.com/locate/jns

Letter to the Editor

Megalencephalic leukoencephalopathy with subcortical cysts caused by compound heterozygous mutations in *MLC1*, in patients with and without subcortical cysts in the brain

Keywords:
Van der Knaap disease
Megalencephalic leukoencephalopathy
Subcortical cysts
MLC1 mutation
MRI
Astrocytes

To the Editor,

Megalencephalic leukoencephalopathy with subcortical cysts (MLC) is a rare hereditary disorder characterized by infantile-onset macrocephaly and a gradual onset of progressive neurological symptoms including ataxia, spasticity, and mild mental decline [1]. As the name of the disorder suggests, patients with MLC invariably had subcortical cysts in the anterior temporal region of the brain [1].

Mutations in two different genes, *MLC1* and *GLIALCAM*, may cause MLC [1,2]. Homozygous or compound heterozygous mutations of *MLC1* were reportedly found in approximately 75% of MLC patients. MLC1 is a plasma membrane protein expressed in the brain and is mainly localized in astrocyte–astrocyte junctions and Bergmann glial cells [3,4]. Although pathophysiological functions of the MLC1 protein remain to be fully elucidated, this protein may be involved in ion transport and water homeostasis [1,5].

In this manuscript, we report on two adult MLC patients who had compound heterozygous mutations, p.Ser93Leu/Ala275Asp, in the *MLC1* gene with and without subcortical cysts in the brain. These findings are important for making an accurate diagnosis of this disease.

1. Case report

A 21-year-old female patient (case 1) was the second child to healthy and non-consanguineous parents. Her birth weight, length, and head circumference were 2988 g (25th–75th percentile), 51 cm (5th–95th percentile), and 34.5 cm (25th–75th percentile), respectively. Her head circumference was 43.5 cm (more than 95th percentile) at 3 months of age, which indicated mild macrocephaly. She rolled over and controlled her head at 4 and 8 months of age, respectively. She walked alone at 16 months of age, but with some difficulty. She showed a gait disturbance at 2.5 years of age and lost the ability to walk and sit unsupported at 3 years of age. Generalized clonic–tonic seizures occurred at 3 years of age and continued until 9 years of age. She was treated with sodium valproate. Brain magnetic resonance imaging (MRI) at 3 years old revealed extensive bilaterally symmetrical white matter changes. She was undiagnosed at that time. Her symptoms progressed gradually. At 21 years of age, she had dysarthria, spasticity, and ataxia. Mental impairment was not observed. Her mini-mental state examination (MMSE) score was 29/30. Brain MRI revealed a diffuse high intensity in the cerebral white matter on fluid-attenuated inversion recovery (FLAIR) images; subcortical cysts were not found in all sections (axial, coronal, sagittal image) in the brain (Fig. 1A-F).

Her younger sister, an 18-year-old female patient (case 2), had been previously diagnosed as having unclassified leukoencephalopathy. Her birth weight, length, and head circumference were 2904 g (25th–75th percentile), 48 cm (25th–75th percentile), and 31 cm (5th–95th percentile), respectively. She rolled over and controlled her head at 5 and 8 months of age, respectively. She walked alone at 18 months of age but fell down easily. She lost the ability to walk and sit unsupported at 2 years of age. At 18 years of age, she also had dysarthria, spasticity, and ataxia without mental impairment. Her MMSE score was 28/30. Brain MRI FLAIR images revealed a diffuse high intensity in the cerebral white matter, with subcortical cysts in the bilateral anterior temporal region (Fig. 1G-J).

We analyzed the *MLC1* cDNA from peripheral leukocytes by using sequence analysis [6] in case 1, case 2, and their parents after we had obtained informed consent. Case 1 and case 2 had compound heterozygous mutations, c. 393C > T (p.Ser93Leu) in exon 4 and c. 823C > A (p.Ala275Asp) in exon 10. Their father had a heterozygous p.Ala275Asp mutation, and their mother had a heterozygous p.Ser93Leu mutation. On the basis of these genetic analysis results, we diagnosed the sisters as having MLC.

2. Discussion

Here, we described two Japanese sisters affected with MLC that was caused by compound heterozygous mutations, p.Ser93Leu/Ala275Asp, in the *MLC1* gene. *MLC1* p.Ser93Leu and p.Ala275Asp mutations were frequently found, especially in Japanese MLC patients [6–9]. Although these two sisters with MLC caused by the same compound heterozygous mutations had similar clinical disease courses and symptoms, subcortical cysts occurred in the brain of only one patient (case 2).

As the name of the disorder suggests, the presence of subcortical cysts in the anterior temporal region, and frequently also in the frontal and parietal regions, is a hallmark of MLC [1]. We did not find any cysts, however, in one MLC patient (case 1). To the best of our knowledge, this patient (case 1) is the first MLC case without subcortical cysts findings in MRI. This patient (case 1) with leukoencephalopathy did not receive a definitive diagnosis until she was 21 years old because

Abbreviations: MLC, megalencephalic leukoencephalopathy with subcortical cysts; MRI, magnetic resonance imaging; FLAIR, fluid-attenuated inversion recovery.

http://dx.doi.org/10.1016/j.jns.2015.03.010

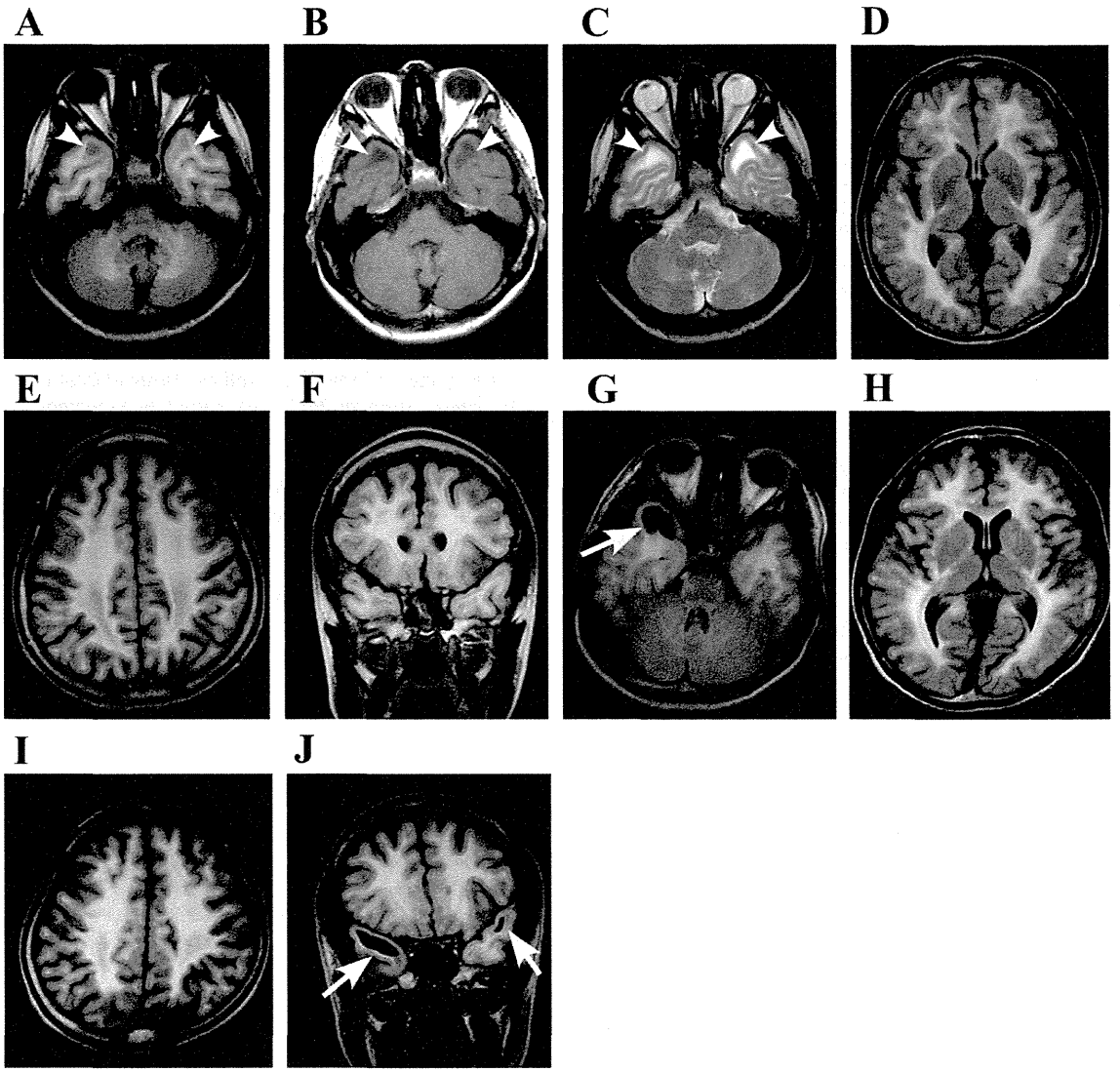

Fig. 1. Brain MRI images of the two adult sisters with MLC. (A–F) Case 1 (II-2). (G–J) Case 2 (II-3). (A, D–J) FLAIR images. (B) T1-weighted image. (C) T2-weighted image. Arrows point to subcortical cysts in the anterior temporal region; the arrowheads indicate anterior temporal lesions without cystic changes in MRI.

her brain MRI did not show the typical subcortical cyst findings. MRI findings in her younger sister (case 2) provided an important clue to her definitive diagnosis. As clinicians attempting to make an accurate diagnosis of MLC, we should understand that certain MLC patients may not have subcortical cysts in the brain.

Via careful evaluation of the FLAIR images, we found small lesions which were isointense with the cortex in the white matter of the anterior temporal region in case 1 (Fig. 1C). These lesions were low intensity in T1-weighted image and high intensity in T2-weighted image. Van der Knaap et al. reported that MLC patients had large numbers of microscopic vacuoles in the white matter based on histopathological examinations [10]. The anterior temporal lesions which were isointense with the cortex without cysts in the FLAIR images may have microscopic vacuoles in the white matter. Since subcortical cysts in MLC might change in size and number over time, subcortical cysts could have been present on earlier MRIs in the case 1. Also, longitudinal follow-up evaluation of this MRI finding should be performed.

In conclusion, in this report, we described two adult sisters with MLC caused by compound heterozygous mutations of *MLC1*, one sister with and one sister without subcortical cysts in the brain. We should thus include MLC in the differential diagnosis of leukoencephalopathy, even in adult patients without subcortical cysts.

Declaration of conflict of interest

The authors declare no conflicts of interest.

Acknowledgments

We would like to thank all members of Department of Neurology, Kumamoto Saisyunsou National Hospital, for helping with the collection of clinical data. We are indebted to Ms. Judith B. Gandy for providing professional English editing of the manuscript.

References

[1] van der Knaap MS, Boor I, Estévez R. Megalencephalic leukoencephalopathy with subcortical cysts: chronic white matter oedema due to a defect in brain ion and water homoeostasis. Lancet Neurol 2012;11:973–85.
[2] López-Hernández T, Ridder MC, Montolio M, Capdevila-Nortes X, Polder E, Sirisi S, et al. Mutant GlialCAM causes megalencephalic leukoencephalopathy with subcortical cysts, benign familial macrocephaly, and macrocephaly with retardation and autism. Am J Hum Genet 2011;88:422–32.
[3] Boor PK, de Groot K, Waisfisz Q, Kamphorst W, Oudejans CB, Powers JM, et al. MLC1: a novel protein in distal astroglial processes. J Neuropathol Exp Neurol 2005;64:412–9.
[4] Teijido O, Martínez A, Pusch M, Zorzano A, Soriano E, Del Río JA, et al. Localization and functional analyses of the MLC1 protein involved in megalencephalic leukoencephalopathy with subcortical cysts. Hum Mol Genet 2004;13:2581–94.

[5] Schmitt A, Gofferje V, Weber M, Meyer J, Mössner R, Lesch KP. The brain-specific protein MLC1 implicated in megalencephalic leukoencephalopathy with subcortical cysts is expressed in glial cells in the murine brain. Glia 2003;44:283–95.
[6] Shimada S, Shimojima K, Masuda T, Nakayama Y, Kohji T, Tsukamoto H, et al. *MLC1* mutations in Japanese patients with megalencephalic leukoencephalopathy with subcortical cysts. Hum Genome Var 2014;1:14019.
[7] Montagna G, Teijido O, Eymard-Pierre E, Muraki K, Cohen B, Loizzo A, et al. Vacuolating megalencephalic leukoencephalopathy with subcortical cysts: functional studies of novel variants in *MLC1*. Hum Mutat 2006;27:292.
[8] Itoh N, Maeda M, Naito Y, Narita Y, Kuzuhara S. An adult case of megalencephalic leukoencephalopathy with subcortical cysts with S93L mutation in MLC1 gene: a case report and diffusion MRI. Eur Neurol 2006;56:243–5.
[9] Koyama S, Kawanami T, Arawaka S, Wada M, Kato T. A Japanese adult case of megalencephalic leukoencephalopathy with subcortical cysts with a good long-term prognosis. Intern Med 2012;51:503–6.
[10] van der Knaap MS, Barth PG, Vrensen GF, Valk J. Histopathology of an infantile-onset spongiform leukoencephalopathy with a discrepantly mild clinical course. Acta Neuropathol 1996;92:206–12.

Teruaki Masuda
Department of Neurology, National Hospital Organization, Kumamoto Saisyunsou Hospital, 2659 Suya, Koshi City, Kumamoto 861-1196, Japan
Department of Neurology, Graduate School of Medical Sciences, Kumamoto University, 1-1-1 Honjo, Chuo-ku, Kumamoto 860-8556, Japan

Mitsuharu Ueda
Department of Neurology, Graduate School of Medical Sciences, Kumamoto University, 1-1-1 Honjo, Chuo-ku, Kumamoto 860-8556, Japan
Corresponding author. Tel.: +81 96 373 5893; fax: +81 96 373 5895.
E-mail address: mitt@rb3.so-net.ne.jp.

Hidetsugu Ueyama
Department of Neurology, National Hospital Organization, Kumamoto Saisyunsou Hospital, 2659 Suya, Koshi City, Kumamoto 861-1196, Japan

Shino Shimada
Tokyo Women's Medical University Institute for Integrated Medical Sciences, 8-1 Kawata-cho, Shinjuku-ku, Tokyo, 162-8666, Japan

Masatoshi Ishizaki
Department of Neurology, National Hospital Organization, Kumamoto Saisyunsou Hospital, 2659 Suya, Koshi City, Kumamoto 861-1196, Japan

Shigehiro Imamura
Department of Neurology, National Hospital Organization, Kumamoto Saisyunsou Hospital, 2659 Suya, Koshi City, Kumamoto 861-1196, Japan

Toshiyuki Yamamoto
Tokyo Women's Medical University Institute for Integrated Medical Sciences, 8-1 Kawata-cho, Shinjuku-ku, Tokyo, 162-8666, Japan

Yukio Ando
Department of Neurology, Graduate School of Medical Sciences, Kumamoto University, 1-1-1 Honjo, Chuo-ku, Kumamoto 860-8556, Japan

30 January 2015

European Journal of Medical Genetics 58 (2015) 492–496

Contents lists available at ScienceDirect

European Journal of Medical Genetics

journal homepage: http://www.elsevier.com/locate/ejmg

Clinical research

Leukoencephalopathy associated with 11q24 deletion involving the gene encoding hepatic and glial cell adhesion molecule in two patients

Toshiyuki Yamamoto [a, b, *], Shino Shimada [a, b], Keiko Shimojima [a], Noriko Sangu [a], Shinsuke Ninomiya [c], Masaya Kubota [d]

[a] Tokyo Women's Medical University Institute for Integrated Medical Sciences, Tokyo, Japan
[b] Department of Pediatrics, Tokyo Women's Medical University, Tokyo, Japan
[c] Department of Clinical Genetics, Kurashiki Central Hospital, Kurashiki, Japan
[d] Division of Neurology, National Center for Child Health and Development, Tokyo, Japan

ARTICLE INFO

Article history:
Received 8 February 2015
Accepted 15 June 2015
Available online 17 July 2015

Keywords:
Megalencephalic leukoencephalopathy with subcortical cysts type 2 (MLC2)
Hepatic and glial cell adhesion molecule (*HEPACAM*)
11q24
Microdeletion
Jacobsen syndrome

ABSTRACT

Leukoencephalopathies are heterogeneous entities with white matter abnormalities. Mutations of the gene encoding hepatic and glial cell adhesion molecule (*HEPACAM*) located on 11q24 are related to one of the leukoencephalopathies: megalencephalic leukoencephalopathy with subcortical cysts type 2 (MLC2). Genomic copy number aberrations were analyzed by microarray comparative hybridization for two patients. One patient who presented with abnormal intensity of the white matter had been previously been diagnosed with the typical genotype and phenotype of Jacobsen syndrome due to an 11q subtelomere deletion, which was further characterized here. In a second patient who exhibited the characteristic finding of leukoencephalopathy, an interstitial deletion of 11q24 was also identified. *HEPACAM* was involved in both deletions. We therefore suggest that haploinsufficiency of *HEPACAM*, a gene previously associated with the features of *MLC2* and located on the overlapping deletion region between the two patients, might be related to the observed white matter abnormalities.

1. Introduction

Leukoencephalopathies are heterogeneous entities characterized by white matter abnormalities (Schiffmann and van der Knaap, 2009). Leukoencephalopathies are generally diagnosed on the basis of their clinical course and neurological findings; however, the patterns of the neuroradiological findings serve as critical elements for ascertaining the specific diagnosis or disease classification (Schiffmann and van der Knaap, 2009). Megalencephalic leukoencephalopathy with subcortical cysts (MLC, MIM #604004) is one type of leukoencephalopathy wherein patients show early onset macrocephaly and delayed-onset neurological deterioration (van der Knaap et al., 1995). Typical patients with MLC show characteristic neuroradiological findings with subcortical cysts in the anterior-temporal region and/or in the frontoparietal region (van der Knaap et al., 2012). Cases of leukoencephalopathy associated with typical findings are relatively easily diagnosed, and 75% of patients with MLC show mutations in *MLC1* (MIM #605908), which is a major gene responsible for MLC that is located on chromosome 22q13.33 (Leegwater et al., 2001). Such molecular genetic evaluation is often required for the final diagnosis (Shimada et al., 2014). The remaining 25% of the patients manifesting the features of MLC show no mutation in *MLC1*, indicating genetic heterogeneity within the leukoencephalopathies. In 2011, the gene encoding the hepatic and glial cell adhesion molecule (*HEPACAM*, MIM #611642) was identified as the second gene associated with MLC features (Arnedo et al., 2014; Lopez-Hernandez et al., 2011a). HEPACAM and MLC1 both localize in axons and colocalize in the junctions between astrocytes, and HEPACAM has been shown to be required as a chaperon for proper localization of MLC1 and activation of volume-regulated anion currents (Capdevila-Nortes et al., 2013; Lopez-Hernandez et al., 2011b).

In this study, we identified two patients with white matter abnormalities associated with partial deletions of chromosome 11. We found that the shortest region of overlap (SRO) of both patients

* Corresponding author. Tokyo Women's Medical University Institute for Integrated Medical Sciences, 8-1 Kawada-cho, Shinjuku-ward, Tokyo 162-8666, Japan.
E-mail address: yamamoto.toshiyuki@twmu.ac.jp (T. Yamamoto).

http://dx.doi.org/10.1016/j.ejmg.2015.06.008
1769-7212/

included the *HEPACAM* locus. In addition, we discuss the functional relevance of haploinsufficiency of *HEPACAM* in these two patients in association with leukoencephalopathies.

2. Methods

This study was approved by the ethics committee in Tokyo Women's Medical University. After obtaining written informed consents from the patients' families, blood samples were obtained from the patients. Chromosomal microarray testing was performed using the Agilent 60K Human Genome CGH Microarray platform (Agilent Technologies, Santa Clara, CA, USA) according to the method described previously (Yamamoto et al., 2011, 2014). Sanger sequencing analysis for *MLC1* and for five genes encoding subunits of the eukaryotic translation initiation factor 2B (*EIF2B1*, *EIF2B2*, *EIF2B3*, *EIF2B4*, and *EIF2B5*) was performed for patient 2 in accordance with our previous studies (Shimada et al., 2012, 2014, 2015). The respective *HEPACAM* sequences were also analyzed by Sanger sequencing for both patients 1 and 2.

3. Results

3.1. Molecular cytogenetic analyses

The two patients reported in this study showed genomic copy number losses in 11q (Fig. 1). Patient 1 showed a subtelomeric deletion of 11q [arr 11q23.3q25(120,930,746–134,868,407) × 1]. The parents of this patient declined to be genotyped. Patient 2 showed an interstitial deletion of 11q [arr 11q23.3q24.2(119,982,356–125,310,469) × 1]. This region was not deleted in either parent of this patient, indicating *de novo* occurrence in patient 2. Additionally, patient 2 did not show any mutation in the coding regions of *MLC1*, *EIF2B1*, *EIF2B2*, *EIF2B3*, *EIF2B4*, and *EIF2B5*. No mutations were identified in the remaining allele of *HEPACAM* in either patient.

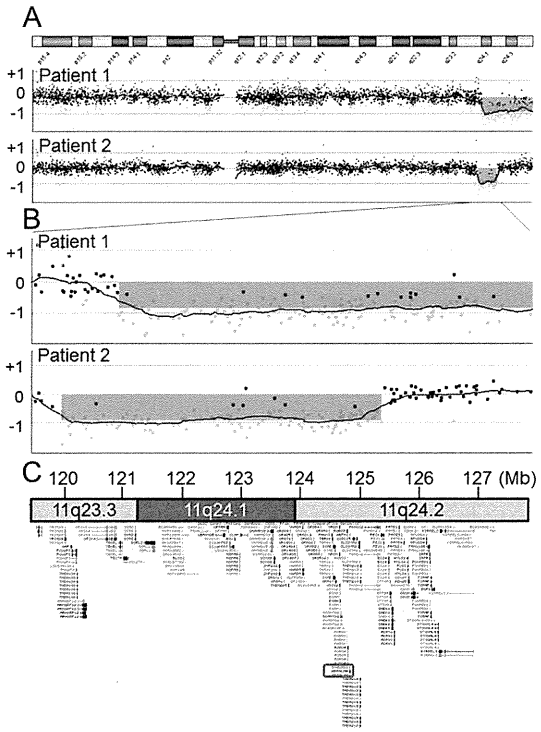

Fig. 1. Genome map of 11q and the results of chromosomal microarray testing. (A) The Chromosome View shows genomic copy number losses in the 11q24 regions in both patients. (B) The shortest region of overlap (SRO) is expanded in the Gene View. (C) Genome map in the same scale as shown in B. *HEPACAM* (red rectangle) is included in the SRO. (For interpretation of the references to colour in this figure legend, the reader is referred to the web version of this article.)

3.2. Patient reports

3.2.1. Patient 1

A 5-year-old girl was born with a birth weight of 1744 g (<3rd centile), a length of 41 cm (<3rd centile), and an occipitofrontal circumference (OFC) of 29.5 cm (3^{rd}–10th centile) at 37 weeks of gestation. Her Apgar score was 5/9 at 1/5 min. After birth, petechial spots were noted on her entire body. Blood examination revealed a low concentration of platelets (17,000/μl). No visceral anomaly was noted. In infancy, she showed delayed growth and development. She started walking without support at the age of 3 years and 5 months. At the age of 3 years and 8 months, her height was 84.5 cm (<3rd centile) and weight was 12.3 kg (10^{th}–25th centile). At that time, brain magnetic resonance imaging (MRI) revealed signal abnormalities in the white matter, predominantly in the deep white matter of the bilateral occipital lobes and faintly in the subcortical regions (Fig. 2). Conventional chromosomal analysis revealed an abnormal karyotype of 46,XX,del(11) (q23), indicating Jacobsen syndrome. Because the clinical features of the patient were compatible with those of Jacobsen syndrome, clinical diagnosis was confirmed.

At present, she still has not spoken meaningful words. The patient has a round face, short neck, bilateral ptosis, long philtrum, and thin upper vermilion. Laboratory examination has revealed her peripheral platelet level in the range of 10,000–80,000/μl.

3.2.2. Patient 2

A 20-month-old boy was born with a birth weight of 3105 g (50^{th}–75th centile), a length of 49.4 cm (50^{th}–75th centile), and an OFC of 36.0 cm (>97th centile) at 41 weeks of gestation, suggesting prenatal macrocephaly. He showed mild psychomotor developmental delay and could stand-up with support at 15 months of age. At present, he can walk with support and can speak only some decipherable words. He shows no distinctive features except for left ptosis and right cryptorchidism. His OFC is 49 cm (50^{th}–75th centile), indicating improvement upon his initial macrocephaly. Brain MRI examination at 20 months of age revealed signal abnormalities remarkably in the subcortical regions rather than in the deep white matter (Fig. 2).

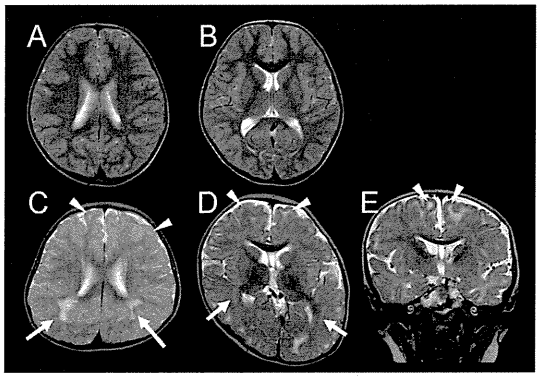

Fig. 2. Brain MRI findings of the patients reported in this study. (A and B) The T2-weighted axial images of a normally developing 4-year-old boy, who was examined for the aim of the disease screening for epilepsy, with normal MRI results. (C) The T2-weighted axial image of patient 1 examined at 3 years and 8 months of age. (D, E) The T2-weighted axial (D) and coronal (E) images of patient 2 examined at 20 months of age. Compared to the normal control (A, B), both patients show T2-high intensities in their deep (arrows) and subcortical (arrow heads) white matter.

Table 1
Gene information included in the deletion region of the patients.

Gene symbol	Gene/Locus MIM number	Description	Position[a]	Phenotype MIM number	Phenotype	Deletion region of the patients
						Patient 2
TRIM29	#610658	tripartite motif containing 29	119,981,994–119,992,701			
OAF		OAF homolog (Drosophila)	120,081,747–120,100,650			
POU2F3	#607394	POU class 2 homeobox 3	120,107,349–120,190,653			
TMEM136		transmembrane protein 136	120,195,838–120,204,388			
ARHGEF12	#604763	Rho guanine nucleotide exchange factor (GEF) 12	120,207,618–120,360,645			
GRIK4	#600282	glutamate receptor, ionotropic, kainate 4	120,530,978–120,856,969			
TBCEL	#610451	tubulin folding cofactor E-like	120,894,803–120,960,354			
TECTA	#602574	tectorin alpha	120,973,375–121,061,515	#601543	Deafness, autosomal dominant 8/12	Patient 1
				#603629	Deafness, autosomal recessive 21	
SC5D	#602286	sterol-C5-desaturase	121,163,388–121,184,119	#607330	Lathosterolosis	
SORL1	#602005	sortilin-related receptor, L(DLR class) A repeats containing	121,322,912–121,504,471	#104300	Association with Alzheimer disease	
BLID	#608853	BH3-like motif containing, cell death inducer	121,986,062–121,986,923			
UBASH3B	#609201	ubiquitin associated and SH3 domain containing B	122,526,398–122,685,187			
CRTAM	#612597	cytotoxic and regulatory T cell molecule	122,709,255–122,743,347			
C11orf63		chromosome 11 open reading frame 63	122,753,236–122,830,430			
BSX	#611074	brain-specific homeobox	122,848,357–122,852,379			
HSPA8	#600816	heat shock 70 kDa protein 8	122,928,200–122,931,094			
CLMP	#611693	CXADR-like membrane protein	122,943,033–123,066,007	#615237	Congenital short bowel syndrome	
GRAMD1B		GRAM domain containing 1B	123,396,528–123,493,518			
SCN3B	#608214	sodium channel, voltage-gated, type III, beta subunit	123,499,895–123,525,315	#613120	Atrial fibrillation, familial, 16	
				#613120	Brugada syndrome 7	
ZNF202	#603430	zinc finger protein 202	123,594,997–123,612,363			
OR6X1		olfactory receptor, family 6, subfamily X, member 1	123,624,288–123,625,226			
TMEM225		transmembrane protein 225	123,753,633–123,756,340			
OR8D4		olfactory receptor, family 8, subfamily D, member 4	123,777,139–123,778,083			
OR4D5		olfactory receptor, family 4, subfamily D, member 5	123,810,324–123,811,280			
OR6T1		olfactory receptor, family 6, subfamily T, member 1	123,813,574–123,814,545			
OR10S1		olfactory receptor, family 10, subfamily S, member 1	123,847,403–123,848,398			
OR10G4		olfactory receptor, family 10, subfamily G, member 4	123,886,282–123,887,217			
OR10G9		olfactory receptor, family 10, subfamily G, member 9	123,893,720–123,894,655			
OR10G8		olfactory receptor, family 10, subfamily G, member 8	123,900,330–123,901,265			
OR10G7		olfactory receptor, family 10, subfamily G, member 7	123,908,773–123,909,708			
VWA5A	#602929	Willebrand factor A domain containing 5A	123,986,111–124,017,618			
OLFR959		NI	124,029,125–124,029,838			
OR10D3		NI	124,055,975–124,056,912			
OR8G2		olfactory receptor, family 8, subfamily G, member 2	124,095,398–124,096,312			
OR8G1		olfactory receptor, family 8, subfamily G, member 1	124,120,423–124,135,763			
OR8D1		olfactory receptor, family 8, subfamily D, member 1	124,179,736–124,180,662			
OR8D2		olfactory receptor, family 8, subfamily D, member 2	124,189,158–124,190,093			
OR8B2		olfactory receptor, family 8, subfamily B, member 2	124,252,298–124,253,239			
OR8B3		olfactory receptor, family 8, subfamily B, member 3	124,266,306–124,267,247			
OR8B4		olfactory receptor, family 8, subfamily B, member 4	124,293,838–124,294,767			
OR8B8		olfactory receptor, family 8, subfamily B, member 8	124,310,046–124,310,981			
OR8B12		olfactory receptor, family 8, subfamily B, member 12	124,412,618–124,413,550			
OR8A1		olfactory receptor, family 8, subfamily A, member 1	124,439,965–124,440,945			
PANX3	#608422	pannexin 3	124,481,453–124,490,251			
TBRG1	#610614	transforming growth factor beta regulator 1	124,492,742–124,505,822			
SIAE	#610079	sialic acid acetylesterase	124,505,685–124,543,777	#613551	Autoimmune disease susceptibility	
SPA17	#608621	sperm autoantigenic protein 17	124,543,740–124,564,687			
NRGN	#602350	neurogranin (protein kinase C substrate, RC3)	124,609,829–124,617,102			
VSIG2	#606011	V-set and immunoglobulin domain containing 2	124,617,370–124,622,109			
ESAM	#614281	endothelial cell adhesion molecule	124,623,019–124,632,223			
MSANTD2		Myb/SANT-like DNA-binding domain containing 2	124,636,394–124,670,299			
ROBO3	#608630	roundabout, axon guidance receptor, homolog 3 (Drosophila)	124,735,305–124,751,370	#607313	Gaze palsy, horizontal, with progressive scoliosis	

ROBO4	#607528	roundabout, axon guidance receptor, homolog 4 (Drosophila)	124,754,114–124,767,831			
HEPN1	#611641	hepatocellular carcinoma, down-regulated 1	124,789,146–124,790,573			
HEPACAM	#611642	hepatic and glial cell adhesion molecule	124,789,146–124,806,308	#613925	Megalencephalic leukoencephalopathy with subcortical cysts 2A	
				#613926	Megalencephalic leukoencephalopathy with subcortical cysts 2B, remitting, with or without mental retardation	
CCDC15		coiled-coil domain containing 15	124,824,017–124,911,385			
SLC37A2		solute carrier family 37 (glycerol-3-phosphate transporter), member 2	124,933,013–124,960,412			
TMEM218		transmembrane protein 218	124,964,266–124,981,604			
PKNOX2	#613066	PBX/knotted 1 homeobox 2	125,034,559–125,303,285			

[a] Genomic position on the chromosome 11 referring to the GRCh37 build reference sequence (hg19); NI, no information.

4. Discussion

In this study, we identified two overlapping chromosomal deletions of 11q associated with white matter abnormalities. Patient 1 showed a subtelomeric deletion of 11q, which is a typical pattern for Jacobsen syndrome. Patients with typical features of Jacobsen syndrome show intellectual disability, short stature, congenital heart defects, thrombocytopenia, and characteristic facial features (Grossfeld et al., 2004; Mattina et al., 2009; Takahashi et al., 2012). Although patient 1 did not show congenital heart defects, the incidence of congenital heart defects in Jacobsen syndrome is not 100% (Wenger et al., 2006). Therefore, clinical features of patient 1 fulfilled the diagnostic criteria for Jacobsen syndrome. Patient 2 showed an interstitial deletion of 11q. Although this patient showed mild developmental delay, he exhibited no other clinical feature distinctive of Jacobsen syndrome. Therefore, patient 2 did not satisfy the diagnostic criteria for this syndrome (Mattina et al., 2009).

Both patients showed neuroradiological abnormalities in the deep and subcortical white matter regions, albeit with different patterns. In patient 1, the main white matter abnormality is observed in the deep white matter, especially in the bilateral occipital lobes, as detected by the T2-weigthed MRI (Fig. 2C). In addition to that, signal abnormalities can be detected also in the subcortical white matter regions. In patient 2, white matter abnormalities are remarkable in the subcortical white matter regions rather than in the deep white matter regions (Fig. 2). Although subcortical cysts were not clearly detected in both patients, the distribution of white matter abnormalities was similar to that seen in the early stage of MLC. Macrocephaly observed in early infantile period of patient 2 is also a suggestive feature of MLC.

We identified a 5.3 Mb region of 11q23.3q24.2 that was deleted in patient 2. Of the genes included in the deletion region, nine genes are registered as disease-causing genes in the database online Mendelian inheritance in men (OMIM), i.e., *ARHGEF12*, *TECTA*, *SC5D*, *SORL1*, *CLMP*, *SCN3B*, *SIAE*, *ROBO3*, and *HEPACAM* (Table 1). Among these, *HEPACAM* has been shown to be associated with megalencephalic leukoencephalopathy with subcortical cysts-2A (MLC2A; MIM# 613925) and B (MLC2B; MIM# 613926) (Lopez-Hernandez et al., 2011a). Furthermore, *HEPACAM* mutations have been shown to exert novel, dual effects including both autosomal recessive (MLC2A) and autosomal dominant (MLC2B) patterns (Arnedo et al., 2014). Patients with *HEPACAM* mutations in an autosomal recessive fashion show classical phenotypes with infantile-onset macrocephaly, delayed-onset motor deterioration, epilepsy, and cognitive decline of variable severity, which are associated with white matter abnormalities (MLC2A) (Lopez-Hernandez et al., 2011a). In comparison, patients with *HEPACAM* mutations inherited in an autosomal dominant fashion have also been reported who show macrocephaly within the first year of life; however, the motor capabilities in these patients were rarely impaired. Furthermore, white matter abnormalities detected upon initial examination of these patients showed improvement upon follow-up; this pattern is classified as MLC2B (Arnedo et al., 2014). Dominantly inherited *HEPACAM* mutations have been reported to often cause benign familial macrocephaly or macrocephaly with intellectual disability and/or autism. However, because the previously reported *HEPACAM* mutations related to MLC2B consisted of missense mutations in the specific domain required for interaction with *MLC1* (Lopez-Hernandez et al., 2011a), it is reasonable to suspect that the underlying mechanism of MLC2B in these patients might be related to dominant-negative effects. Macrocephaly has also been reported in one of the parents of a patient with MLC2A who carried a loss-of-function mutation (Lopez-Hernandez et al., 2011a), indicating that both *HEPACAM* haploinsufficiency as well

as mutation might cause macrocephaly. Because we were unable to identify a *HEPACAM* mutation in the remaining allele of patient 2, we assume that haploinsufficiency of *HEPACAM* is the only mechanism related to macrocephaly and white matter abnormalities in this patient. Macrocephaly of patient 2 was identified at birth, but has improved at 20 months; it is unclear whether the white matter abnormalities might improve as well, as do those of patients with *HEPACAM* mutations rather than deletions.

Although most of the deletion regions identified in patients with Jacobsen syndrome include *HEPACAM*, no previous patient with Jacobsen syndrome has been reported to show an MLC-like phenotype. However, some of the previously reported patients with Jacobsen syndrome have shown related findings. For example, Ono et al. reported two patients with 11q deletions associated with delayed myelination, suspected by the abnormal signal intensities revealed by MRI (Ono et al., 1994). In addition, Grossfeld et al. reported that abnormal brain imaging findings were identified in 24/47 (51%) of patients with Jacobsen syndrome (Grossfeld et al., 2004). The result of the present study provide additional insight into these findings: we identified a patient with Jacobsen syndrome (patient 1) associated with white matter abnormalities, although the identified distributions were different from those observed in patient 2. *HEPACAM* was included in the SRO of both patients, we considered that haploinsufficiency of *HEPACAM* might therefore cause white matter abnormalities to varying degrees. We suggest that the improvement of phenotype overtime, or a low penetrance of white matter abnormalities consequent to *HEPACAM* deletion might, among other factors, contribute to the lack of descriptions of MLC-like phenotypes in patients with Jacobsen syndrome to date.

In addition, it is likely that the developmental delay observed in patient 2 could have been modified by the loss of neighboring genes included in the deletion region. In 2009, Coldren et al. analyzed genotype–phenotype correlations for 14 patients with Jacobsen syndrome and suggested that two genes, the brain-specific homeobox gene (*BSX*) and the neurogranin gene (*NRGN*), might be possible candidate genes for global and selective deficits in neurocognitive functions (Coldren et al., 2009). Because both of these genes are also included in the SRO identified in this study (Table 1), haploinsufficiencies of these two genes in particular might have modified neurodevelopment in patient 2 as well.

In conclusion, we report the characterization of two patients with white matter abnormalities in association with 11q24 deletions involving *HEPACAM*. This finding suggests that haploinsufficiency of *HEPACAM* might be related to white matter abnormalities. Further studies are required to obtain more information on white matter abnormalities in patients with 11q24 deletions in order to confirm the results of this study.

Conflict of interest

The authors have no conflict of interests to declare.

Acknowledgment

We thank the patients and their families for cooperation in this study. We would like to acknowledge the Collaborative Research Supporting Committee of the Japanese Society of Child Neurology (14-3) for promoting this study. This work was supported by a Grant-in-Aid for Scientific Research from Health Labor Sciences Research Grants from the Ministry of Health, Labor, and Welfare, Japan (T.Y.).

References

Arnedo, T., Aiello, C., Jeworutzki, E., Dentici, M.L., Uziel, G., et al., 2014. Expanding the spectrum of megalencephalic leukoencephalopathy with subcortical cysts in two patients with GLIALCAM mutations. Neurogenetics 15, 41–48.

Capdevila-Nortes, X., Lopez-Hernandez, T., Apaja, P.M., Lopez de Heredia, M., Sirisi, S., et al., 2013. Insights into MLC pathogenesis: GlialCAM is an MLC1 chaperone required for proper activation of volume-regulated anion currents. Hum. Mol. Genet. 22, 4405–4416.

Coldren, C.D., Lai, Z., Shragg, P., Rossi, E., Glidewell, S.C., et al., 2009. Chromosomal microarray mapping suggests a role for BSX and neurogranin in neurocognitive and behavioral defects in the 11q terminal deletion disorder (Jacobsen syndrome). Neurogenetics 10, 89–95.

Grossfeld, P.D., Mattina, T., Lai, Z., Favier, R., Jones, K.L., et al., 2004. The 11q terminal deletion disorder: a prospective study of 110 cases. Am. J. Med. Genet. A 129A, 51–61.

Leegwater, P.A., Yuan, B.Q., van der Steen, J., Mulders, J., Konst, A.A., et al., 2001. Mutations of MLC1 (KIAA0027), encoding a putative membrane protein, cause megalencephalic leukoencephalopathy with subcortical cysts. Am. J. Hum. Genet. 68, 831–838.

Lopez-Hernandez, T., Ridder, M.C., Montolio, M., Capdevila-Nortes, X., Polder, E., et al., 2011. Mutant GlialCAM causes megalencephalic leukoencephalopathy with subcortical cysts, benign familial macrocephaly, and macrocephaly with retardation and autism. Am. J. Hum. Genet. 88, 422–432.

Lopez-Hernandez, T., Sirisi, S., Capdevila-Nortes, X., Montolio, M., Fernandez-Duenas, V., et al., 2011. Molecular mechanisms of MLC1 and GLIALCAM mutations in megalencephalic leukoencephalopathy with subcortical cysts. Hum. Mol. Genet. 20, 3266–3277.

Mattina, T., Perrotta, C.S., Grossfeld, P., 2009. Jacobsen syndrome. Orphanet J. Rare Dis. 4, 9.

Ono, J., Harada, K., Hasegawa, T., Sakurai, K., Kodaka, R., et al., 1994. Central nervous system abnormalities in chromosome deletion at 11q23. Clin. Genet. 45, 325–329.

Schiffmann, R., van der Knaap, M.S., 2009. Invited article: an MRI-based approach to the diagnosis of white matter disorders. Neurology 72, 750–759.

Shimada, S., Miya, K., Oda, N., Watanabe, Y., Kumada, T., et al., 2012. An unmasked mutation of EIF2B2 due to submicroscopic deletion of 14q24.3 in a patient with vanishing white matter disease. Am. J. Med. Genet. A 158A, 1771–1777.

Shimada, S., Shimojima, K., Masuda, T., Nakayama, Y., Kohji, T., et al., 2014. MLC1 mutations in Japanese patients with megalencephalic leukoencephalopathy with subcortical cysts. Hum. Genome Var. 1, 14019.

Shimada, S., Shimojima, K., Sangu, N., Hoshino, A., Hachiya, Y., et al., 2015. Mutations in the genes encoding eukaryotic translation initiation factor 2B in Japanese patients with vanishing white matter disease. Brain Dev. http://dx.doi.org/10.1016/j.braindev.2015.03.003 **(in press).**

Takahashi, I., Takahashi, T., Sawada, K., Shimojima, K., Yamamoto, T., 2012. Jacobsen syndrome due to an unbalanced translocation between 11q23 and 22q11.2 identified at age 40 years. Am. J. Med. Genet. A 158A, 220–223.

van der Knaap, M.S., Barth, P.G., Stroink, H., van Nieuwenhuizen, O., Arts, W.F., et al., 1995. Leukoencephalopathy with swelling and a discrepantly mild clinical course in eight children. Ann. Neurol. 37, 324–334.

van der Knaap, M.S., Boor, I., Estevez, R., 2012. Megalencephalic leukoencephalopathy with subcortical cysts: chronic white matter oedema due to a defect in brain ion and water homoeostasis. Lancet Neurol. 11, 973–985.

Wenger, S.L., Grossfeld, P.D., Siu, B.L., Coad, J.E., Keller, F.G., et al., 2006. Molecular characterization of an 11q interstitial deletion in a patient with the clinical features of Jacobsen syndrome. Am. J. Med. Genet. A 140, 704–708.

Yamamoto, T., Shimojima, K., Nishizawa, T., Matsuo, M., Ito, M., et al., 2011. Clinical manifestations of the deletion of down syndrome critical region including DYRK1A and KCNJ6. Am. J. Med. Genet. A 155A, 113–119.

Yamamoto, T., Wilsdon, A., Joss, S., Isidor, B., Erlandsson, A., et al., 2014. An emerging phenotype of Xq22 microdeletions in females with severe intellectual disability, hypotonia and behavioral abnormalities. J. Hum. Genet. 59, 300–306.

ELSEVIER

Brain & Development 37 (2015) 988–989

BRAIN & DEVELOPMENT
Official Journal of the Japanese Society of Child Neurology

www.elsevier.com/locate/braindev

Letter to the Editor

Comment on "Delayed myelination is not a constant feature of Allan–Herndon–Dudley syndrome: Report of a new case and review of the literature" by Azzolini S et al. Brain & Development 2014;36:716–720

Dear the editor of Brain and Development, we read a manuscript by Azzolini et al. with a great interest, because we have been participating in the clinical and genetic diagnosis of patients with congenital hypomyelinating disorders [1] by establishing a research network for Pelizaeus–Merzbacher disease (PMD) and related disorders. There, we have many opportunities in evaluating the radiological findings of the patients suspected to have hypomyelinating disorders including Allan–Herndon–Dudley syndrome (AHDS) [2,3]. Compared to other congenital hypomyelination disorders, radiological findings of AHDS patients are different in that the magnetic resonance imagings (MRIs) in infancy show lack of myelin, which improve over time. Therefore, it would rather be termed as delayed myelination than hypomyelination [4].

Azzolini et al. reported a male patient (as assumed by the description "he") [1]. The patient showed severe psychomotor developmental delay. The thyroid function test showed an elevated free T3 level. Molecular testing identified one nucleotide insertion in *SLC16A2*. Together, they concluded that this patient has AHDS. Finally, they reported that the patient show "normal" myelination by MRI [1], while delayed myelination is commonly observed in AHDS patients, as we also reported previously [2,3].

We suggest that the description of "normal" MRIs presented by Azzolini et al. is inappropriate [1]. For comparison, we presented a reference MRIs observed in a normally developing 12-month-old boy (Fig. 1). As we can see, the T1-weighted image shows high intensity in the white matter, which is almost the same pattern observed in adults. T2-weighted image clearly shows low intensity in the subcortical regions, except for the temporal lobe, the latest to myelinate (not shown). Compared to these, the MRIs reported by Azzolini et al. shows apparently lower intensity (than normal) on T1-weighted image, and higher intensity on T2-weighted image in most of the subcortical regions [1]. We would rather consider this finding as delayed myelination and is typical for AHDS.

Fig. 1. Brain MRI findings in a normally developing 12-month-old boy. T1 – (left) and T2 – (right) weighted axial images the slice matched with that reported by Azzolini et al. The subcortical regions are enough high and low in T1- and T2-weighted images, respectively. This patient was examined for the aim of the disease screening for epilepsy and the results came out as normal.

http://dx.doi.org/10.1016/j.braindev.2015.03.007

As Azzolini et al. reported [1], there are three case reports showing "normal" myelination in the literature; however, these cases were examined in either too early (at 3 months) [5,6] or too late stage (13 years) [7] for the evaluation of the delayed myelination in AHDS. Therefore, it is possible that delayed myelination could not be captured in those cases simply because of the timing of MRI examination. Altogether, it would be improper to conclude that the delayed myelination is not constant feature for AHDS. We suggest that adequate timing is important to access MRIs in the evaluation of delayed myelination in AHDS patients [4].

References

[1] Azzolini S, Nosadini M, Balzarin M, Sartori S, Suppiej A, Mardari R, et al. Delayed myelination is not a constant feature of Allan–Herndon–Dudley syndrome: report of a new case and review of the literature. Brain Dev 2014;36:716–20.
[2] Kobayashi S, Onuma A, Inui T, Wakusawa K, Tanaka S, Shimojima K, et al. Clinical course and images of four familial cases of Allan–Herndon–Dudley syndrome with a novel monocarboxylate transporter 8 gene mutation. Pediatr Neurol 2014;51:414–6.
[3] Yamamoto T, Shimojima K, Umemura A, Uematsu M, Nakayama T, Inoue K. *SLC16A2* mutations in two Japanese patients with Allan–Herndon–Dudley syndrome. Human Genome Variation 2014;1:14010.
[4] van der Knaap MS, Wolf NI. Hypomyelination versus delayed myelination. Ann Neurol 2010;68:115.
[5] Dumitrescu AM, Liao XH, Best TB, Brockmann K, Refetoff S. A novel syndrome combining thyroid and neurological abnormalities is associated with mutations in a monocarboxylate transporter gene. Am J Hum Genet 2004;74:168–75.
[6] Holden KR, Zuniga OF, May MM, Su H, Molinero MR, Rogers RC, et al. X-linked MCT8 gene mutations: characterization of the pediatric neurologic phenotype. J Child Neurol 2005;20:852–7.
[7] Schwartz CE, May MM, Carpenter NJ, Rogers RC, Martin J, Bialer MG, et al. Allan–Herndon–Dudley syndrome and the monocarboxylate transporter 8 (MCT8) gene. Am J Hum Genet 2005;77:41–53.

Toshiyuki Yamamoto *
Tokyo Women's Medical University Institute for Integrated Medical Sciences, 8-1 Kawada-cho, Shinjuku-ward, Tokyo 162-8666, Japan
** Tel.: +81 3 3353 8111x24013; fax: +81 3 3353 6793.*
E-mail address: yamamoto.toshiyuki@twmu.ac.jp

Jun-ichi Takanashi
Department of Pediatric Neurology, Tokyo Women's Medical University Yachiyo Medical Center, Yachiyo, Japan

Kenji Kurosawa
Division of Genetics, Kanagawa Children's Medical Center, Yokohama, Japan

Kimiko Deguchi
Deguchi Pediatric Clinic, Nagasaki, Japan

Hitoshi Osaka
Department of Pediatrics, Jichi Medical University, Shimotsuke, Japan

Ken Inoue
National Institute of Neuroscience, National Center for Neurology and Psychiatry, Kodaira, Japan